

Experimental study on the hydraulic fracture propagation in shale

Shuai Heng^{1,2,*}, Chunhe Yang³, Lei Wang³ and J. J. K. Daemen⁴

¹School of Energy Science and Engineering, Henan Polytechnic University, Jiaozuo, Henan Province 454000, China

²Collaborative Innovation Center of Coalbed Methane and Shale Gas for Central Plains Economic Zone, Jiaozuo, Henan Province 454000, China

³State Key Laboratory of Geomechanics and Geotechnical Engineering, Institute of Rock and Soil Mechanics, Chinese Academy of Sciences, Wuhan, Hubei 430071, China

⁴Machay School of Earth Sciences and Engineering, University of Nevada, Reno, NV, USA

To realize the control on geometry of fracture network and improve the individual well production of shale gas reservoirs, hydraulic fracturing simulation tests of shale outcrops for horizontal well were carried out. This was based on an established true triaxial hydraulic fracturing simulation test system, to analyse the propagation and formation of a complex fracture network. The results show that the typical severe fluctuation of pump pressure during extension, is an obvious feature of hydraulic fracturing by Stimulated Reservoir Volume (SRV). Due to the large size and abundant natural fractures in shale specimens, the acoustic emission (AE) energy is weak during propagation of hydraulic fractures. However, fracture propagation can still be effectively determined to some extent, although relatively few AE events are detected. Hydraulic fractures from horizontal well initiate approximately along the maximal *in situ* stress. But the fractures gradually deviate from the orientation when extending. Branching, re-orientation or penetrating bedding planes and then interconnecting with natural fractures or weak beddings are the main mechanisms of the formation of complicated fracture networks.

Keywords: Fracture propagation, fracture network, hydraulic fracturing, shale, stimulated reservoir volume.

OWING to the low porosity and ultra-low permeability of shale matrix, stimulated reservoir volume (SRV) is regarded as an essential stimulation technology to achieve industrial gas production¹⁻³. The understanding of the propagation mechanism of fractures in shale with SRV can contribute to guide fracturing design and help control the fracture geometry, thus increasing the ultimate recovery and single well production. Many factors affect the geometry of post-fracturing network. But the key factors controlling the fracture geometry are the rock brittleness, difference of horizontal *in situ* stresses, sedimentary bedding and natural fracture system⁴⁻⁶. However, the fracturing effect in shale gas reservoirs in 1500–4000 m deep, cannot be effectively identified, as accurate and

effective field monitoring methods are lacking^{7,8}. Therefore, the laboratory hydraulic fracturing simulation experiment is an important and accurate tool to study fracture propagation and formation mechanism.

Many fracturing simulation experiments were carried out on coal^{9,10}, cement blocks^{11,12} and sandstones^{13,14}. The propagation mechanisms in these rocks under certain conditions were revealed. Some studies have also been conducted to analyse the influence of natural fractures on hydraulic fracture propagation^{13,15,16}. But the propagation is quite different from that in shale, due to the special physical–mechanical properties of shale¹⁷⁻¹⁹. Studies have recognized the existence of a complex fracture network in shale fracturing, but the propagation mechanism is still not clear²⁰. True triaxial hydraulic fracturing simulation tests were carried out on shale outcrops by Zhang *et al.*²¹⁻²⁵, but only a few factors affecting the fracture geometry and growth were investigated. The fracture geometry of post-fracturing was also observed by high-energy CT scanning²²⁻²⁵, but the complicated fracture propagation is still not discussed. A large-scale hydraulic fracturing simulation test system was established by Guo *et al.*²⁵⁻²⁷. The extension and geometry of hydraulic fracture network was explored, and the forming mechanism was preliminarily revealed. Shale outcrops were selected to study the hydraulic fracture extension and the interaction between natural fractures and hydraulic fractures through true triaxial fracturing tests by Hou *et al.*²⁸, but only the hydraulic fracturing with variable pump rates was discussed.

Many attempts have been made to study hydraulic fracture propagation by true triaxial fracturing simulation tests on shale, and several study results have been obtained. But most of them focus on the influence of multiple factors on hydraulic fracture propagation. The fracture geometry of shale with SRV is a complicated fracture network instead of a conventional symmetric bi-wing fracture. The concepts of single bi-wing fracture theory are insufficient to represent the complicated fracture network. Consequently, it is important to understand the formation and propagation of complex fracture network by means of hydraulic fracturing simulation tests to

*For correspondence. (e-mail: shheng@yeah.net)

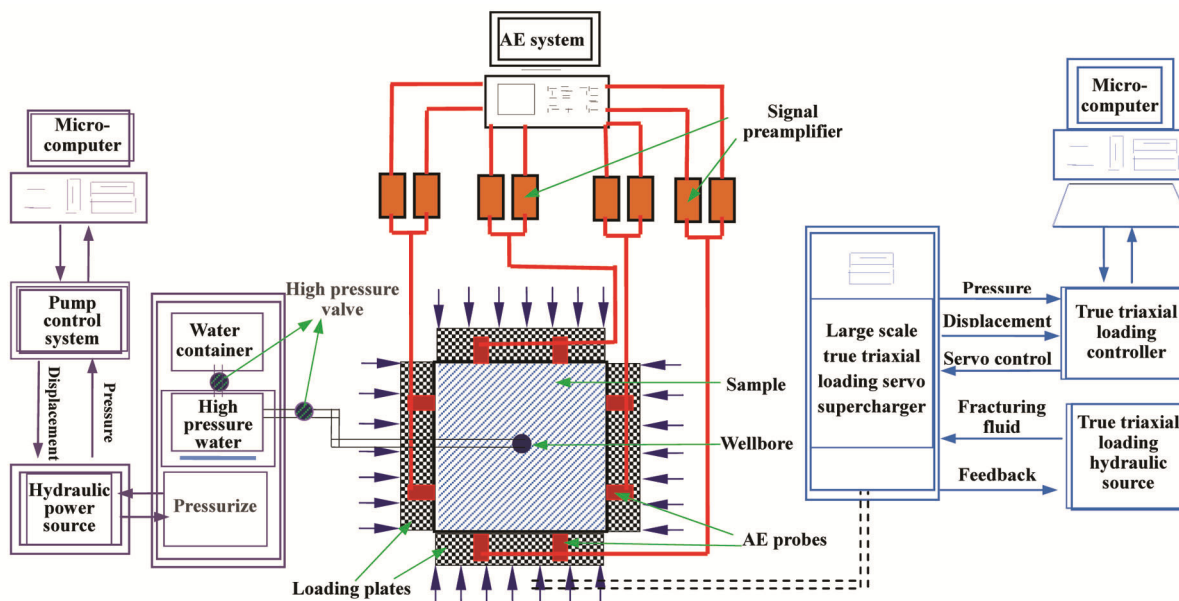


Figure 1. Technical route of true triaxial hydraulic fracturing simulation tests.

formulate the best stimulation strategy for shale gas reservoirs.

In this study, in order to understand the propagation and formation of hydraulic fractures in shale with SRV, large-size true triaxial fracturing simulation tests on shale outcrops were conducted. The propagation and formation of hydraulic fracture network were analysed based on the characteristics of pump pressure curve, monitored AE events and fracture geometry of post-fracturing specimens after cutting. The research findings can provide a theoretical basis and technical support for efficient development of shale gas.

Large scale true triaxial hydraulic fracturing simulation system

A large-scale true triaxial hydraulic fracturing simulation system is developed based on a true triaxial servo loading system, pump pressure servo control system and AE monitoring system. The technical route for hydraulic fracturing simulation tests conducted by this system is shown in Figure 1.

True triaxial servo loading system

The true triaxial servo loading system (Figure 2) is an electro-hydraulic servo control system suitable for simulating the three-dimensional stress state of underground rock. A cubic specimen of 300 to 800 mm in size can be tested by the true triaxial assembly, in which axial loads can be applied by large jacks. The maximum force of 3000 kN can be applied by this system. That is, the three confining stresses can reach up to 33.3 MPa.



Figure 2. Large scale true triaxial servo loading system.

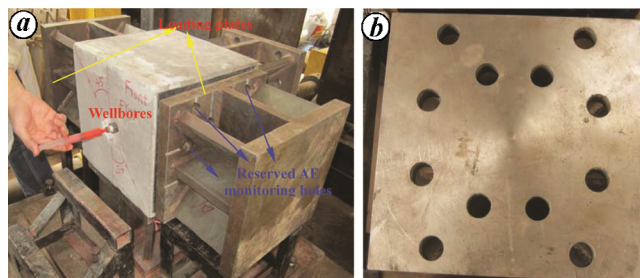


Figure 3. Loading plates and their assembly. a, Assembling process of the loading plates. b, The reserved AE monitoring holes on a loading plate.

In order to monitor the AE events of the specimen, 12 placing holes, with a diameter of 25 mm, were pre-fabricated on the end surface of the loading plate. The position of AE probes can be adjusted according to the AE monitoring results to achieve a better monitoring

Table 1. Technical parameters of the pump pressure servo control system

Technical parameter	Maximum output pressure	Pressure resolution	Pressure accuracy	Available volume of supercharger	Maximum range of displacement sensor	Displacement resolution	Volume resolution	Displacement accuracy
Value	100 (MPa)	0.05 (MPa)	1 (%)	80 (ml)	210 (mm)	0.04 (mm)	0.15 (ml)	1 (%)

**Figure 4.** Pump pressure servo control system.**Figure 6.** Industrial CT of CD-600BXA.

result. The loading plates and their assembly are shown in Figure 3.

Pump pressure servo control system

The pump pressure servo control system is shown in Figure 4. The main technical parameters are presented in Table 1. In order to increase the dynamic response speed of the servo valve and ensure its stability, a high sensitivity electro-hydraulic servo control valve was used and accumulators installed in the inlet and outlet of oil.

AE monitoring system

Initiation and propagation of hydraulic fractures were monitored by the AE monitoring system. Eight AE probes with operating frequency from 15 to 70 kHz and centre frequency of 40 kHz were used. Two AE probes were asymmetrically placed on the four end surfaces parallel to the wellbore axis, as shown in Figure 5. To improve the monitoring, the AE probes and the specimen were bonded with a couplant.

Scanning system of industrial CT

The fracture geometry of specimens pre- and post-fracturing were scanned by the high-energy computed

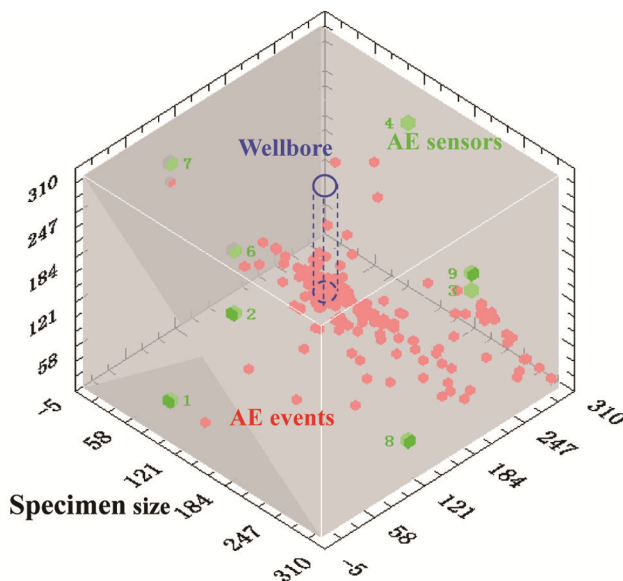
**Figure 5.** Distribution of the eight AE sensors on the sample surfaces parallel to the wellbore axis. The eight green dots represent the location of the AE sensors, the red dots represent the monitored AE signals.

Table 2. Technical parameters of the industrial CT of CD-600BXA

Technical parameter	Energy	Maximum turning diameter of workpiece	Maximum length of workpiece	Spatial resolution	Maximum imaging pixel	Accuracy
Value	6, 4, 2 (MeV)	600 (mm)	1200 (mm)	2.5 (LP/mm)	4096 * 4096 (Pixel * Pixel)	0.02–0.05 (mm)

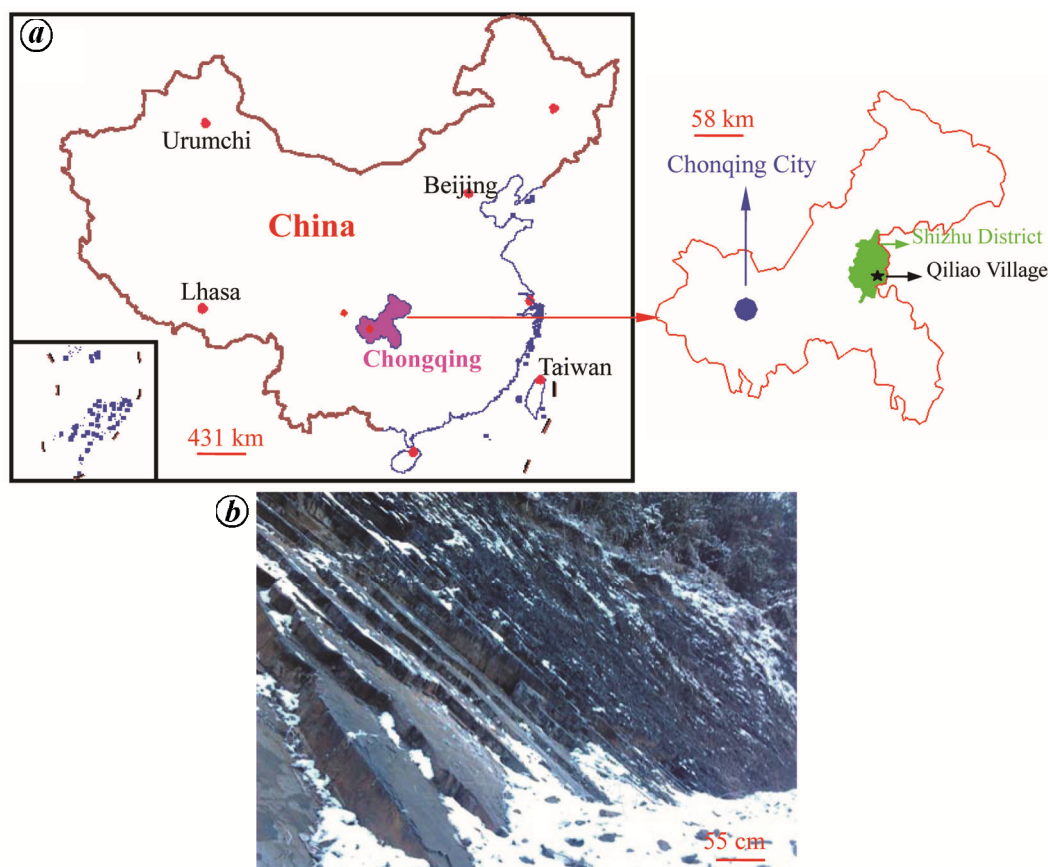


Figure 7. Outcrops of the tested specimens and its geographic position. *a*, Location map of the study area. *b*, Shale outcrops of the Longmaxi Formation where tested specimens were collected.

tomography (CT) scanning system in ICT research center of Chongqing University. The high-energy industrial CT scanning system is shown in Figure 6.

High-energy electronic linear accelerator was used as X-ray source for the industrial CT of CD-600BXA.

The main technical parameters of the system are presented in Table 2.

True triaxial hydraulic fracturing simulation test

Field sampling

As relatively intact larger specimens could not be acquired from shale gas wells, the samples tested were obtained from the outcrops of the Longmaxi Formation in Shizhu County, which is the natural extension of the

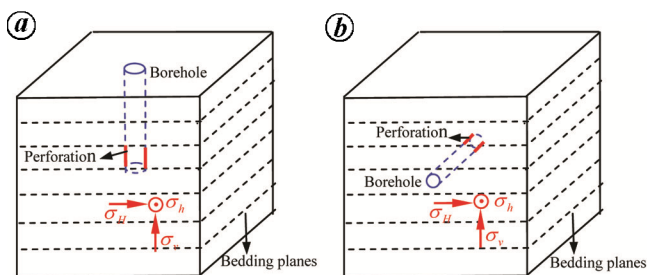
formations in shale gas blocks of Pengshui in Chongqing city of China (Figure 7). During sampling, the weathered rock layer on the surface of the outcrops was first removed. The well-preserved fresh outcrops with relatively small disturbance at the bottom were obtained. The samples obtained were immediately sealed with polyvinyl chloride film to avoid colliding, weathering and wetting-drying cycles in the course of processing and transportation.

Mineral analysis indicated that the mean contents of quartz, clay and carbonate were 55.5%, 6.9% and 10.0% respectively. The content of brittle minerals (quartz) was higher, while the content of clay minerals was relatively low. The mechanical parameters of shale are presented in Table 3. As shown by the brittleness index calculated by Young's modulus–Poisson's ratio method²⁹ and the ratio of uniaxial compressive strength to tensile strength³⁰, the

Table 3. Mechanical properties of shale specimens cored both normal and parallel to bedding

Bedding orientation	Uniaxial compressive strength (MPa)	Young's modulus (GPa)	Poisson's ration	Tensile strength (MPa)	Shear modulus (GPa)
Bedding-normal orientation	118	14.06	0.367	9.89	7.8
Bedding-parallel orientation	118.4	25	0.312	4.3	9.53*

*The shear modulus parallel to the bedding orientation is not an independent elastic parameter, which can be calculated by the equation of $G = E/2(1 + \mu)$ in the bedding-parallel orientation.

**Figure 8.** Symmetrical slotted steel pipe and the simulation casing.**Figure 9.** Schematic diagram of the relative orientation of the borehole axis, beddings and the *in situ* stress. *a*, Vertical well. *b*, Horizontal well.

brittleness indices were 2.89 and 19.72 respectively. Shale can be fractured effectively due to its high brittleness.

Sample preparation

The obtained shale blocks were processed into 300 mm × 300 mm × 300 mm cubes. A circular hole with depth of 170 mm was drilled to simulate the wellbore. The vertical and horizontal wells were simulated by the holes drilled perpendicular and parallel to the beddings respectively. High strength steel tubes with an inside diameter of 15 mm and outside diameter of 20 mm were used to simulate the casing pipes. A 1.5 mm width seam symmetrically cut at a depth of 135 to 165 mm was used to simulate perforations, as shown in Figure 8. The bottom of the steel pipe was welded closed and the female thread at the upper end of the pipe was made to hermetically connect the pipelines of the pump pressure servo control system. The male thread was made to better fix the simulation casing pipe. The casing and the

pre-fabricated hole were sealed by a high strength binder. In order to ensure that the perforation channel was not blocked by the binder, the simulated perforation was filled with cotton yarn from the outside of the tube to the inside. The length of the filled part was equal to that of the simulated perforation, 30 mm. The length of the cotton yarn outside of the casing was kept in the range of 10–15 mm.

The angle between perforation direction and maximum horizontal *in situ* stress was 0°, followed by 30°, 45°, 60° and 90° when a vertical well was simulated. As the three *in situ* stresses were loaded, the vertical *in situ* stress was applied along the borehole axis, perpendicular to the beddings. The minimum and maximum horizontal *in situ* stresses were applied along the direction of beddings, as shown in Figure 9 *a*. When the horizontal well was simulated, the borehole was drilled along the beddings. The minimum horizontal *in situ* stress was applied along the borehole axis, while the vertical *in situ* stress was perpendicular to the beddings, as shown in Figure 9 *b*. During the tests, the applied vertical *in situ* stress, denoted by σ_v was 20 MPa. The applied minimum and maximum horizontal *in situ* stresses denoted by σ_h and σ_H were 17.74 MPa and 19.51 MPa respectively.

Experimental method and procedure

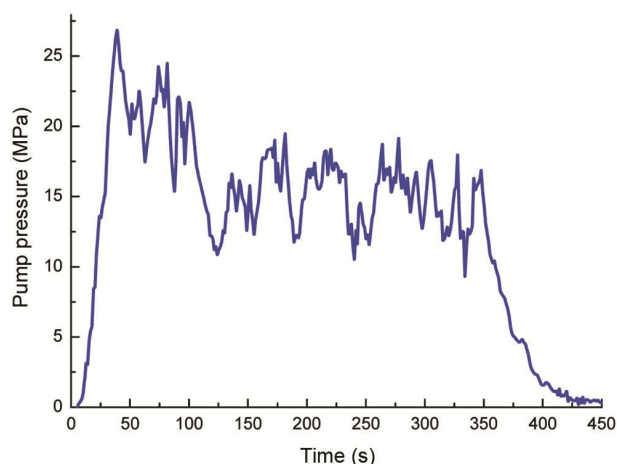
The three-dimensional stress state was simulated by the true triaxial servo loading system. The displacement of fracturing fluid was controlled by the pump pressure servo control system. The initiation and extension of hydraulic fractures were monitored by the AE monitoring system. The fracture geometries of specimens pre- and post-fracturing were observed by high-energy industrial CT scanning. Low viscosity water was used as the fracturing fluid to stimulate the hydraulic fracture propagation. A red colour agent was added to the fracturing fluid as a tracer to visualize the hydraulic fracture propagation.

During test, the pump pressure servo control system and AE monitoring system were started simultaneously, when the three *in situ* stresses were loaded to the desired values. The pump pressure and the AE events were synchronously and constantly acquired by computers. When the test was completed, the fracture geometry of each side of the post-fracturing sample was described first by

Table 4. Test parameters of hydraulic fracturing experiments of shale specimens

Sample number	Triaxial stress (MPa)			Differential coefficient of <i>in situ</i> stress	Simulated well type	Displacement (ml/s)
	σ_v	σ_H	σ_h			
Y-7-6	20	19.51	18.58	0.05	Horizontal well	0.5
Y-7-2	20	19.51	17.74	0.1	Horizontal well	0.5
Y-4-4	20	19.51	16.98	0.15	Horizontal well	0.5
Y-7-3	20	19.51	16.98	0.15	Horizontal well	1
Y-7-4	20	19.51	16.98	0.15	Horizontal well	1
Y-7-5	20	19.51	16.98	0.15	Horizontal well	1.5

The definition of difference coefficient of *in situ* stress is $k = (\sigma_H - \sigma_h) / \sigma_h$. Considering that serious internal damage of specimens may be caused by the loading plate in loading and even failure and cracking may occur, the loaded *in situ* stresses were reduced by the same ratio.

**Figure 10.** Fracture geometry of hydraulic fracturing of shale specimens.**Figure 11.** Pump pressure during a hydraulic fracturing test of shale.

sketching. Then the fracture geometry was observed by the high-energy industrial CT scanning. Finally, the fractured specimens were cut along the traces of the red colour agent, and the hydraulic fracture propagation was described by tracing the red traces.

Propagation of hydraulic fractures from horizontal well

In general, the fracture propagation can be better understood by comparing the CT scanning images of specimens

pre- and post-fracturing and the traces of the red colour agent of specimens post-fracturing. However, given the high scan expenses of the high-energy industrial CT, only a few samples can be scanned before and after fracturing. AE monitoring, which can also better reflect the fracture initiation and propagation, is an important method to study the hydraulic fracture propagation. Therefore, the hydraulic fracture extension in the tests was thoroughly monitored by AE monitoring and tracing the red colour agent. The hydraulic fracture propagation from the horizontal well was mainly analysed in this study, as it is closer to the field situation. The fracturing parameters of some samples are shown in Table 4.

After tests, a relatively complicated fracture network was observed in most samples, as shown in Figure 10 *a* and *b*. The fracture geometry of the specimens in the same batch shows a great difference. A great number of repeated tests is still needed for a better understanding of the hydraulic fracture propagation. Here the propagation of hydraulic fracture was analysed in detail only by one specimen.

Characteristic of the pump pressure curve versus injection time

The pump pressure response versus injection time with the displacement of piston as the control method is plotted in Figure 11. The displacement rate of the piston is 0.25 mm/s, i.e. the displacement of pump pressure is 1 ml/s.

As seen from Figure 11, the pump pressure increased approximately linearly in the early stage. At the injecting time of 40 s, the pump pressure reached the fracturing pressure of 26.88 MPa and initial fractures occurred. When the fracturing fluid flowed into the formed fractures, the pump pressure dropped rapidly. As the pump pressure reduced to about 19 MPa, it decreased slowly, accompanied by jagged fluctuation. The severe pressure fluctuation indicates that a large number of sub-fractures occurred due to the existence of natural fractures or weak beddings, which induced considerable fracturing fluid

loss. Pressure fluctuation is an obvious characteristic of the formation of a fracture network. The pump pressure dropped rapidly again when the injection time was about 350 s. This indicated that hydraulic fractures had extended to the specimen surface and seepage channels had formed. When the pump pressure dropped to a stable value about 1 MPa, the flow channels had been fully formed. Generally, as Figure 11 shows, the extension pressure is lower than the fracture pressure, which corresponds to the theory of fracture mechanics.

AE monitoring of hydraulic fracture propagation

The distribution of monitored AE events of the specimen in three-dimensional space is presented in Figure 12.

Figure 12 indicates that, in general, the number of AE events monitored is relatively low. Due to the large size and abundant micro-fractures in the specimen, the AE energy is pretty weak during fracture propagation. Consequently, it is extremely difficult to monitor the local complicated sub-fractures. The monitored AE events are limited and mainly concentrated around the casing perforation, and reduce as the distance from the perforation increases. However, the spatial distribution of the AE signals can still reflect the hydraulic fracture extension to a large extent. Hence, the hydraulic fracture initiation and propagation was mainly analysed by the spatial distribution of the monitored AE events in this study.

In order to reflect fractures of the hydraulic geometry more intuitively, the hydraulic fracture propagation is analysed mainly from the plane normal to the borehole axis. Figure 13 presents the distribution of cumulative AE

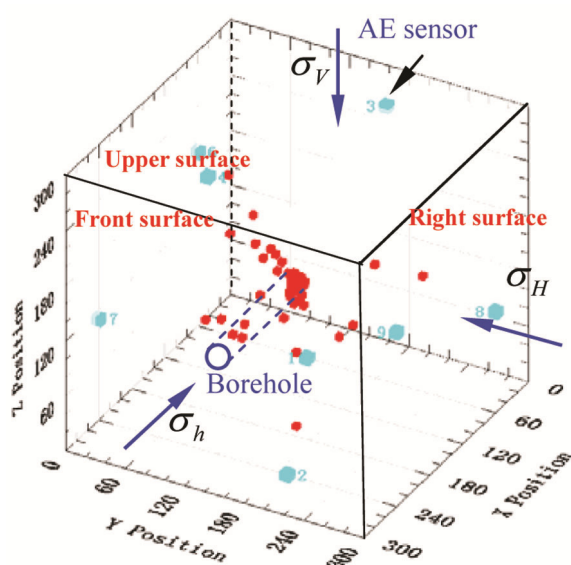


Figure 12. Distribution of the AE events of the fracturing specimen in three-dimensional space.

events and the schematic diagram of hydraulic fractures propagation at the injection time of 50, 150, 250, 350 and 450 s respectively.

As seen from Figure 13, the extension of hydraulic fractures from the stimulated horizontal well is roughly as follows:

(1) Figure 13 *a* shows the hydraulic fracture initiated from the well-bore approximately along the greatest *in situ* stress. The oblique main fracture (denoted by fracture 1) occurred due to the gradual diversion of the hydraulic fracture away from the greatest *in situ* stress during propagation. The offset of the extending path was closely associated with the propagation of tensile-shear fractures induced by beddings.

(2) Comparing AE events in Figure 13 *a* and *b*, it can be seen that a new main fracture was initiated from the borehole wall in extension of fracture 1. The new main fracture was initiated approximately along the greatest *in situ* stress. But the deviation was different from that of the fracture 1. The two main fractures were symmetric about the vertical *in situ* stress, which further indicated that the fracture path deflection was probably caused by the tensile-shear fracture.

(3) As seen from Figure 13 *b* and *c*, approximately vertical re-orientation occurred when the fracture 1 interacted with weak beddings at the injection time of 150 s. An obvious diverting fracture can be observed when the injection time was 250 s. But owing to the lower cohesive strength of beddings, AE events were rarely monitored when the hydraulic fractures extended along the bedding. This further indicated that the ability to resist fracture propagation of bedding planes was weak and lower energy was needed when hydraulic fractures propagated along the beddings.

(4) As shown in Figure 13 *d*, due to the existence of weak beddings, fracture 1 branched to bedding fractures during the propagation of fracture 3. The branching fracture expressed as fracture 4 in Figure 13 *d* also extended along beddings. The upper wing of fracture 1 is re-oriented in weak beddings and then propagated along the beddings. A few AE signals were still monitored during extension of the fracture 2 in the upper part of the beddings. This illustrates that the cohesive strength of the local beddings was stronger than that of the fracture 1. The fracture 2 penetrated the beddings and continued to extend along the maximal *in situ* stress.

(5) As indicated in Figure 13 *e*, the fracture 5 extended along beddings formed by orientation of the upper wing of the fracture 1 and penetrated the fracture 2. The fracture network throughout the specimen has preliminarily been formed.

Overall, hydraulic fracture was initiated from the well-bore approximately along the maximal *in situ* stress. The fracture path deflected continuously and deviated from the maximal *in situ* stress in extension, due to the presence of weak beddings. The complicated fracture network

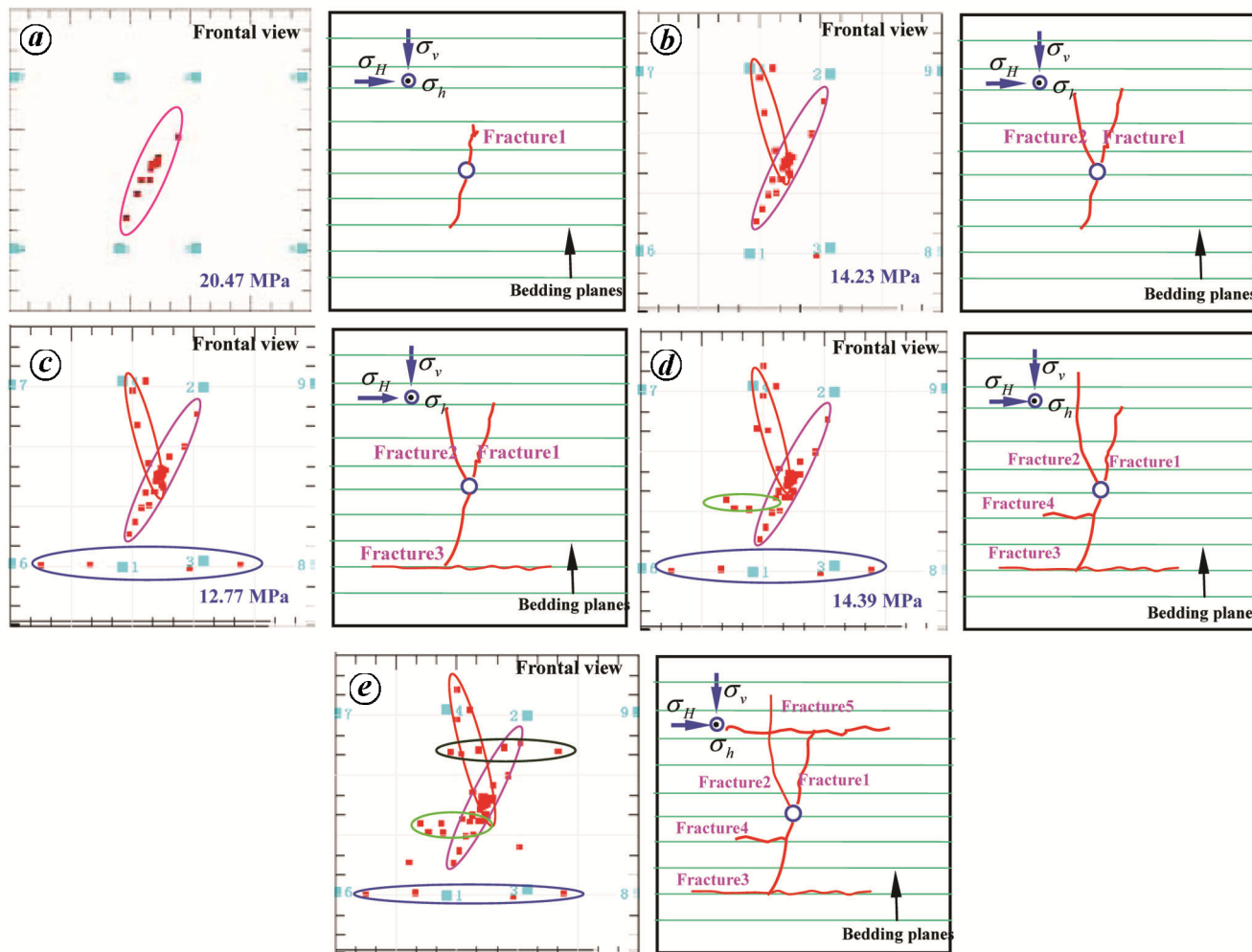


Figure 13. Spatial distribution of AE events and schematic diagrams of the propagation of hydraulic fractures from the plane normal to the bore-hole axis. *a*, Injecting time of: *a*, 50 s; *b*, 150 s; *c*, 250 s; *d*, 350 s; *e*, 450 s.

was formed by the branching, re-orienting of hydraulic fractures or penetrating beddings and then interconnecting with natural fractures or weak beddings, when the fractures extended to a weak bedding.

Almost no AE events were monitored when hydraulic fracture propagated along natural fractures, but the extension of hydraulic fracture along natural fractures was obtained by analogy with that of weak beddings. As a matter of fact, the extension and geometry of fracture in hydraulic fracturing are more complicated than those observed in Figures 14 and 15, owing to well developed stratification and natural fractures.

Specimen cut after fracturing

To determine the effectiveness of hydraulic fracture propagation by AE monitoring, the fractured samples were cut along the traces of the red colour agent. The extension and spatial distribution of hydraulic fractures were observed by the distribution of the red colour agent.

The fracture geometry normal to the beddings are presented in Figure 14.

As seen from Figure 14, the fracture geometry monitored by AE monitoring is roughly the same as that observed from the specimen cut after fracturing. AE monitoring is effective in monitoring the propagation of hydraulic fractures. However, some fractures still cannot be monitored, which may be related to the weaker energy of AE events or abundant natural fractures in the specimen.

The extension of hydraulic fractures observed by cutting the specimen post-fracturing is shown in Figure 15.

As seen from Figure 15, the hydraulic fracture approximately initiated and extended along the maximal *in situ* stress. The criss-crossed fracture network throughout the specimen was formed by branching, re-orienting of hydraulic fractures or penetrating beddings and then interconnecting with natural fractures or weak beddings, when the fractures extended perpendicular to a weak bedding. The SRV of shale is achieved by repeated branching,

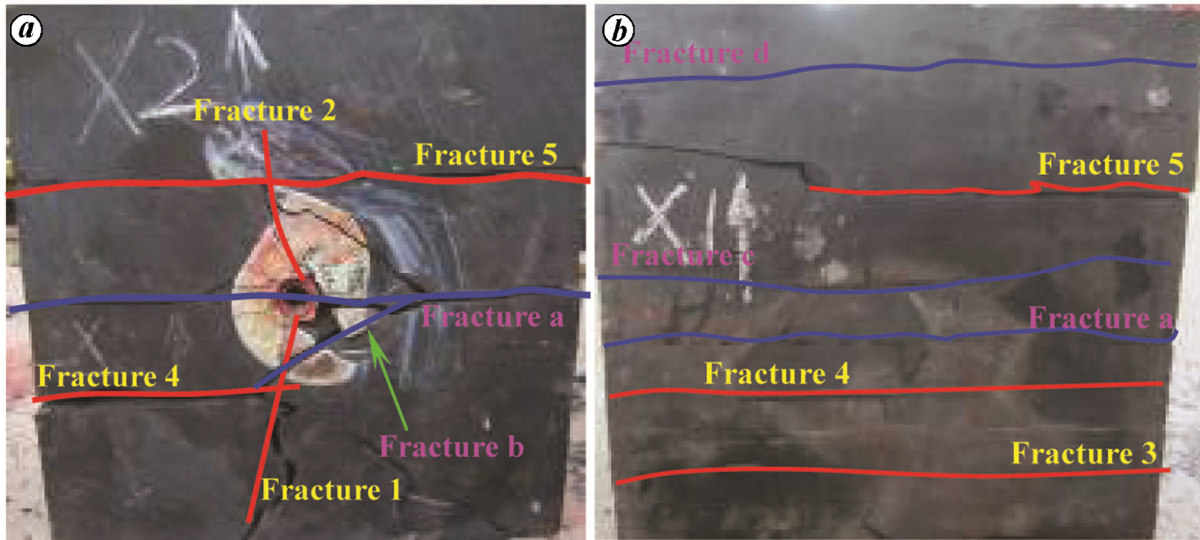


Figure 14. Fracture geometry of post-fracturing sample normal to the beddings. *a*, Frontal view. *b*, Left view (the frontal view and left view can be distinguished from Figure 12).

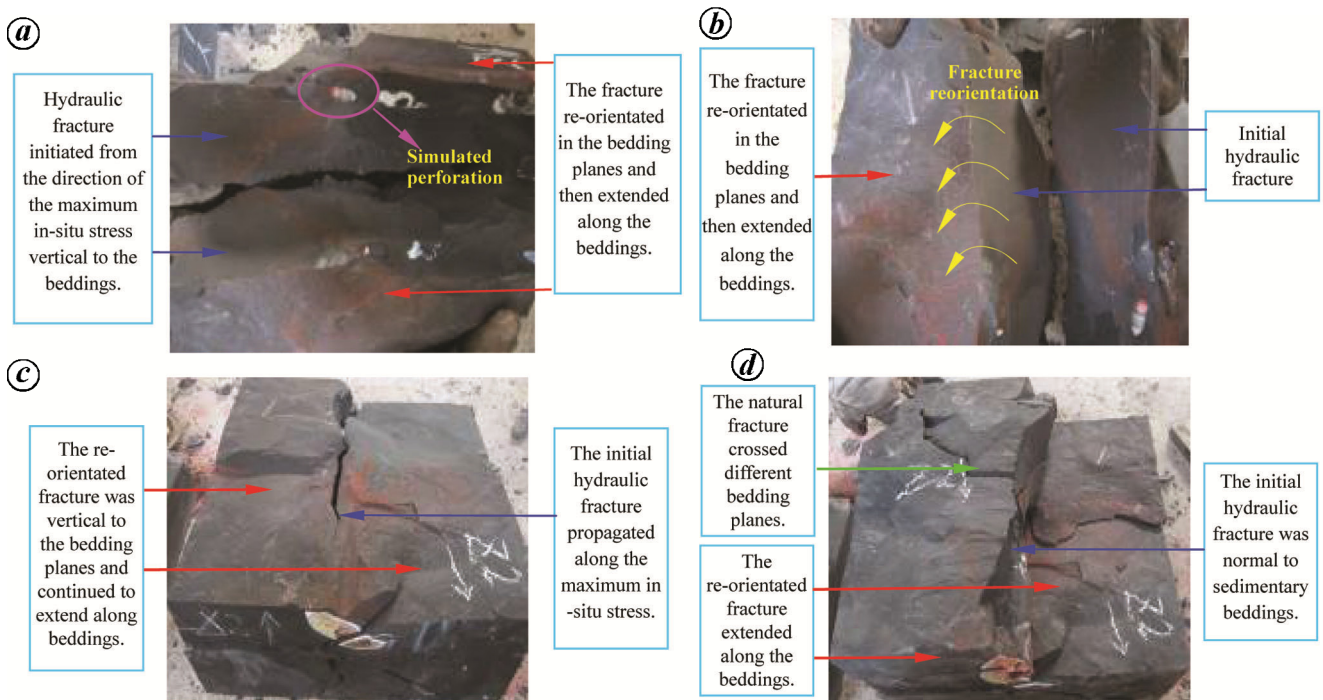


Figure 15. Fractures observed on the specimen cut after hydraulic fracturing. *a*, Hydraulic fracture initiated from the maximum *in situ* stress. *b*, Hydraulic fracture re-orientated in weak beddings. *c*, Initial hydraulic fracture intersected with fracture re-orientated in the beddings. *d*, Initial fracture is perpendicular to the fractures extending along the bedding planes.

re-orienting and penetrating of hydraulic fractures in bedding or natural fractures during extending.

Discussion

Conducting *in situ* hydraulic fracturing tests in shale gas wells is the most reliable way to determine the geometry and propagation of hydraulic fractures. However, such tests are expensive and yet provide only spot information

for the test depths at drilling locations. Drilling many deep boreholes is impractical at least at present. Thus there exists a need to determine the hydraulic fracture propagation from laboratory simulations. The most important aspect of laboratory simulations and field fracturing is the similarity between the scale models and the prototype; both should have similar geometry, kinematics and boundary conditions. Large samples are needed in laboratory simulations to avoid scale effects^{31,32}.

However, large samples require higher power, higher cost, more space and more auxiliary equipment, which usually makes the tests impossible. But the sample boundary will limit the fracture extension if the sample is too small. Thus, the relatively small sample should be large enough to include features like grains, pores, fissures and natural fractures similar to real reservoirs. Consequently, surface outcrops are usually collected to conduct the simulations, as large enough samples can be obtained. The similarity between the outcrop characteristics and the subsurface geological conditions is the key to understanding whether the study results are effective. The selected outcrop should have similar sedimentary facies, provenance, depositional structure and rock composition compared to the subsurface. But the rock properties, geological conditions and rock mechanics are usually different from that in subsurface. The actual reservoirs, as deep as several kilometers or even deeper, have high temperatures, high pore pressures and high *in situ* stresses. In addition, the grains of different sizes, pores and fractures of various shapes and sizes are presented. It is difficult to recreate the reservoir conditions in the laboratory, but the simulation results can still provide a quantitative reference for subsurface reservoirs.

The temperatures under laboratory conditions are different from the temperatures in subsurface shale gas wells and the difference increases with depth increases. Temperature effect is not considered in the building of the test system because of the complexity of working with high temperature. To address this issue, the temperature of the room housing the system was heated to about 40°C when testing, which may not be a long-term solution. Thus, the study is limited to depths of 1500 m, where the formation temperature is usually about 40°C (ref. 33).

Conclusion

Based on the true triaxial hydraulic fracturing simulation tests of horizontal wells on shale outcrops, the following conclusions are obtained from this study:

(1) The pump pressure increased rapidly in the initial stage. A relatively large number of AE events was monitored when the breakdown pressure was reached. The pump pressure decreased slowly accompanied by jagged fluctuations during the hydraulic fractures extension until the fracture channel fully formed. The typical severe fluctuation of pump pressure, which may be closely related to the formation of fracture network, is an obvious feature of the SRV of shale.

(2) Due to the large size and abundant micro-fractures in specimens, the AE energy is pretty weak during fracture propagation. Therefore, it is extremely difficult to monitor the local complicated sub-fractures. The number of AE events monitored during the test is relatively low.

But the limited AE events can still reflect the extension of hydraulic fracture to a large extent.

(3) The hydraulic fracture from the simulated horizontal well initiated from the borehole wall approximately along the maximal *in situ* stress, deviated from the orientation caused by the continuous fracture path deflection, due to the existence of beddings. The complicated fracture network was formed by branching, re-orienting of hydraulic fractures or penetrating beddings and then interconnecting with natural fractures or weak beddings, when the fractures extended to a weak bedding.

(4) The well-developed beddings, natural fractures and other weak structural planes not only provide essential conditions for oil and gas storage and migration, but also provide a pre-condition for the formation of complex fracture network in fracturing. They also make possible large-scale commercial exploitation of shale gas through horizontal well staged fracturing.

- Clarkson, C. R. *et al.*, Pore structure characterization of North American shale gas reservoirs using USANS/SANS, gas adsorption, and mercury intrusion. *Fuel*, 2013, **103**, 606–616.
- Zou, C. *et al.*, Geological characteristics, formation mechanism and resource potential of shale gas in China. *Petrol. Exp. Dev.*, 2010, **37**(6), 641–653.
- Cipolla, C. L. *et al.*, The relationship between fracture complexity, reservoir properties, and fracture treatment design. In SPE Annual Technical Conference and Exhibition, Society of Petroleum Engineers, 2008.
- King, G. E., Thirty years of gas shale fracturing: what have we learned?. In SPE Annual Technical Conference and Exhibition, Society of Petroleum Engineers, 2010.
- Britt, L. K. and Schoeffler, J., The geomechanics of a shale play: what makes a shale prospective. In SPE Eastern Regional Meeting, Society of Petroleum Engineers, 2009.
- Rickman, R. *et al.*, A practical use of shale petrophysics for stimulation design optimization: All shale plays are not clones of the Barnett Shale. In SPE Annual Technical Conference and Exhibition, Society of Petroleum Engineers, 2008.
- Wang, G.-C., Jiang, R.-Z. and Xu, J.-C., Analysis and advice for shale gas development. *Complex Hydrocarbon Res.*, 2012, **5**(2), 10–14.
- Xie, H.-P. *et al.*, Unconventional theories and strategies for fracturing treatments of shale gas strata. *J. Sichuan Univ.* (Engineering science edition), 2012, **44**(6), 1–6.
- Du, C., Study on theoretics of hydraulic fracturing in coal bed and applications. PhD thesis, China University of Mining and Technology, 2008.
- Bingxiang, H., Research on theory and application of hydraulic fracture weakening for coal-rock mass. *J. China Coal Soc.*, 2010, **35**(10), 1765–1766.
- Beugelsdijk, L. J. L., De Pater, C. J. and Sato, K., Experimental hydraulic fracture propagation in a multi-fractured medium. In SPE Asia Pacific Conference on Integrated Modelling for Asset Management, Society of Petroleum Engineers, 2000.
- Zhou, J. *et al.*, Experiment of propagation mechanism of hydraulic fracture in multi-fracture reservoir. *J. Univ. Petrol. China* (edition of natural science), 2008, **32**(4), 51–54.
- Casas, L. A. *et al.*, Laboratory hydraulic fracturing test on a rock with artificial discontinuities. In SPE Annual Technical Conference and Exhibition, Society of Petroleum Engineers, 2006.
- Damani, A. *et al.*, Mapping of hydraulic fractures under triaxial stress conditions in laboratory experiments using acoustic

- emissions. In SPE Annual Technical Conference and Exhibition, Society of Petroleum Engineers, 2012.
15. Zhou, J., Jin, Y. and Chen, M., Experimental investigation of hydraulic fracturing in random naturally fractured blocks. *Int. J. Rock Mech. Min. Sci.*, 2010, **47**(7), 1193–1199.
 16. Zhou, J. *et al.*, Analysis of fracture propagation behavior and fracture geometry using a tri-axial fracturing system in naturally fractured reservoirs. *Int. J. Rock Mech. Min. Sci.*, 2008, **45**(7), 1143–1152.
 17. Sarout, J. *et al.*, Shale dynamic properties and anisotropy under triaxial loading: Experimental and theoretical investigations. *Phys. Chem. Earth, Parts A/B/C*, 2007, **32**(8), 896–906.
 18. Heng, S. *et al.*, Experimental research on anisotropic properties of shale. *Rock and Soil Mech.*, 2015, **36**(3), 609–616.
 19. Heng, S. *et al.*, Experimental and theoretical study of the anisotropic properties of shale. *Int. J. Rock Mech. Mining Sci.*, 2015, **74**, 58–68.
 20. Weng, X. *et al.*, Modelling of hydraulic-fracture-network propagation in a naturally fractured formation. *SPE Prod. Oper.*, 2011, **26**(04), 368–380.
 21. Xu, Z. *et al.*, Physical simulation of hydraulic fracturing of shale gas reservoir. *Petroleum Drilling Techniques*, 2013, **41**(2), 70–74.
 22. Yushi, Z. *et al.*, Experimental investigation into hydraulic fracture network propagation in gas shales using CT scanning technology. *Rock Mech. Rock Eng.*, 2016, **49**(1), 33–45.
 23. Guo, T. *et al.*, Experimental study of hydraulic fracturing for shale by stimulated reservoir volume. *Fuel*, 2014, **128**, 373–380.
 24. Zhang, S. *et al.*, Fracture propagation mechanism experiment of hydraulic fracturing in natural shale. *Acta Petrolei Sin.*, 2014, **35**(3), 496–503, 518.
 25. Zhang, Y. *et al.*, A study of hydraulic fracture propagation for shale fracturing. *Sci. Technol. Eng.*, 2015, **15**(5), 11–16.
 26. Guo, Y. *et al.*, Research on hydraulic fracturing physical simulation of shale and fracture characterization methods. *Chin. J. Rock Mech. Eng.*, 2014, **33**(1), 52–59.
 27. Heng, S. *et al.*, Experimental study on hydraulic fracture geometry of shale. *Chin. J. Geotechn. Eng.*, 2013, **36**(7), 1243–1251.
 28. Hou, B. *et al.*, Fracturing mechanism of shale gas reservoir with variable pump rates. *Chin. J. Geotechn. Eng.*, 2014, **36**(11), 2149–2152.
 29. Rickman, R. *et al.*, A practical use of shale petrophysics for stimulation design optimization: All shale plays are not clones of the Barnett Shale. In SPE Annual Technical Conference and Exhibition, Society of Petroleum Engineers, 2008.
 30. Goktan, R. M. and Yilmaz, N. G., A new methodology for the analysis of the relationship between rock brittleness index and drag pick cutting efficiency. *J. South Afr. Inst. Min. Metallur.*, 2005, **105**(10), 727.
 31. Yoshinaka, R. *et al.*, Practical determination of mechanical design parameters of intact rock considering scale effect. *Eng. Geol.*, 2008, **96**(3), 173–186.
 32. Illman, W. A., Strong field evidence of directional permeability scale effect in fractured rock. *J. Hydrol.*, 2006, **319**(1), 227–236.
 33. Zhang, G. Q. and Fan, T., A high-stress tri-axial cell with pore pressure for measuring rock properties and simulating hydraulic fracturing. *Measurement*, 2014, **49**, 236–245.
- ACKNOWLEDGEMENTS. We acknowledge financial support from National Science Foundation of China (No. 51574218, No. 51704097) and the Doctor Foundation of Henan Polytechnic University (No. 660207/009).
- Received 2 June 2017; revised accepted 5 March 2018
- doi: 10.18520/cs/v115/i3/465-475